Optical Down-Sampling of Wide-Band Microwave Signals

Paul W. Juodawlkis, *Member, IEEE, Member, OSA*, Jeffrey J. Hargreaves, *Member, IEEE*, Richard D. Younger, Gerard W. Titi, *Member, IEEE*, and Jonathan C. Twichell, *Member, IEEE*

Invited Paper

***Abstract*—Phase-encoded optical sampling allows radio-frequency and microwave signals to be directly down-converted and digitized with high linearity and greater than 60-dB (10-effective-bit) signal-to-noise ratio. Wide-band electrical signals can be processed using relatively low optical sampling rates provided that the instantaneous signal bandwidth is less than the Nyquist sampling bandwidth. We demonstrate the capabilities of this technique by using a 60-MS/s system to down-sample two different FM chirp signals: 1) a baseband (0–250 MHz) linear-chirp waveform and 2) a nonlinear-chirp waveform having a 10-GHz center frequency and a frequency excursion of 1 GHz. We characterize the frequency response of the technique and quantify the analog bandwidth limitation due to the optical pulse width. The 3-dB bandwidth imposed by a 30-ps sampling pulse is shown to be 10.4 GHz. We also investigate the impact of the pulse width on the linearity of the phase-encoded optical sampling technique when it is used to sample high-frequency signals.**

***Index Terms*—Analog-to-digital conversion, electrooptic devices, microwave receivers, optical sampling, pulsed lasers, signal sampling.**

I. Introduction

RAPID improvements in the performance of digital signal-processing hardware are expected to have significant impact on advanced radar, surveillance, and communication systems. The flexibility of the receivers in these systems can be augmented by pushing the analog-to-digital converter (ADC) closer to the antenna and performing more of the receiver functions (e.g., out-of-band rejection, down-conversion, matched filtering, and detection) in the digital domain. The ability to implement these digital-receiver architectures is often limited by the performance of the ADC component. For example, the sampling rates of ADCs having 16, 12, and 8 effective bits are currently limited to around 1 MS/s, 100 MS/s, and 1 GS/s, respectively [1]–[4].

Any sampling system is limited by two distinct bandwidth constraints: the analog bandwidth and the Nyquist bandwidth. The analog bandwidth refers to the effective bandwidth of the analog components prior to the sampling operation. In a conventional electronic receiver, the analog bandwidth is determined by the amplifiers, mixers, and filters that condition the signal between the system input and the sample-and-hold circuit in the ADC. The 3-dB analog bandwidth is the frequency range over which the input signal power is attenuated by less than 3 dB of the maximum signal transmission. The Nyquist bandwidth is equal to half the sampling frequency. A signal with all of its frequency components restricted to the Nyquist bandwidth is uniquely specified by its sampled representation. In a conventional electronic ADC, the analog bandwidth is often limited to a few times the Nyquist bandwidth.

Recently, there has been significant interest in applying optical sampling techniques to extend the performance of electronic ADCs [5]–[9]. In the optical sampling approach described here, a high-speed train of short optical pulses is used to sample an electrical signal via an electrooptic modulator. The optical pulses are converted to electrical signals that are subsequently digitized using electronic quantizers. Advantages of optical sampling relative to electrical sampling include:

1) the timing jitter of modern mode-locked lasers is more than an order of magnitude smaller than that of electronic sampling circuitry [1], [9]–[13];
2) the low dispersion of optical components allows picosecond sampling pulses to be used to attain wide analog bandwidth.

In this paper, we investigate the wide-analog-bandwidth characteristics of the phase-encoded optical sampling technique [5]. We show that the analog bandwidth is limited only by the bandwidth of the optical modulator and the temporal width of the optical pulse. An optical sampling system having 30-MHz Nyquist bandwidth is used to directly down-sample FM chirp signals having total frequency excursions of 250 MHz and 1 GHz. These down-sampled signals are processed digitally to extract high-fidelity information about the linearity of the chirp waveforms.

II. Optical Down-Conversion Techniques

A wide variety of optical down-conversion techniques have been reported in the literature [14]–[22]. Although the down-conversion topologies differ, most of the approaches involve impressing electrical radio-frequency (RF) and

Manuscript received May 4, 2003; revised August 5, 2003. This work was supported by the Defense Advanced Research Projects Agency's Photonic A/D Converter Technology (PACT) program under Air Force Contract F19628-00-C-0002.

The authors are with Lincoln Laboratory, Massachusetts Institute of Technology, Lexington MA 02420-9108 USA (e-mail: juodawlkis@ll.mit.edu).

Digital Object Identifier 10.1109/JLT.2003.821736

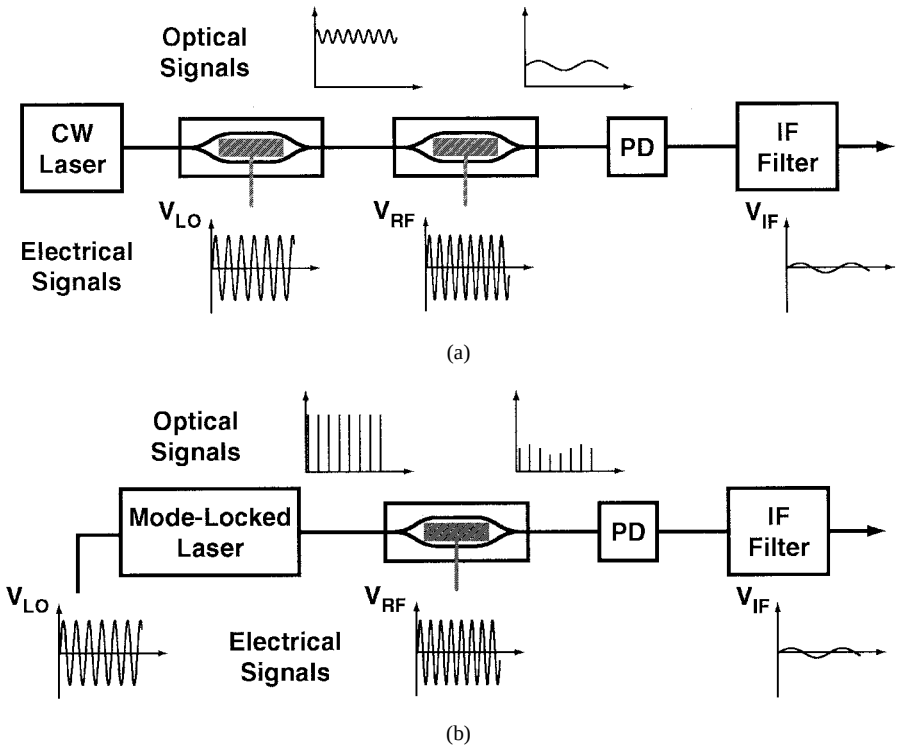

Fig. 1. Optical down-conversion techniques: (a) CW laser and cascaded modulators biased at quadrature and (b) optical down-sampling using a mode-locked laser and a single modulator. PD: photodiode. Note that second modulator output in (a) only shows optical power at the IF frequency for clarity.

local-oscillator (LO) signals onto an optical carrier or carriers, mixing these two signals in a nonlinear medium or device, detecting the mixed signal with a photodetector, and filtering the photodetector output to isolate the desired intermediate-frequency (IF) signal having frequency $f_{\rm IF} = f_{\rm RF} - f_{\rm LO}$. One approach that has been thoroughly investigated uses a continuous-wave (CW) laser and a pair of modulators connected in series and biased at quadrature [Fig. 1(a)] [15]. The first modulator is used to impress the LO signal onto the optical carrier. The second modulator is used to mix the LO-modulated carrier with the RF signal. The overall nonlinear response of the cascaded modulator pair is the product of the sinusoidal transfer characteristics of the individual modulators. When both modulators are biased at quadrature, the cascaded modulator approach does not generate third-order mixing products at frequencies $2f_{\rm RF} \pm f_{\rm LO}$ and $2f_{\rm LO} \pm f_{\rm RF}$. However, when the RF signal contains multiple frequencies, intermodulation products will be generated by the sinusoidal nonlinearity of the second modulator. The main disadvantage of this and many other optical down-conversion techniques is low conversion efficiency. The conversion efficiency can be improved through the use of monolithically cascaded modulators and impedance matching circuits [20], optical amplification, and differential detection [17]. The use of differential detection was also shown to reject both the laser relative intensity noise (RIN) and added noise from an optical amplifier.

The modulated-LO optical signal can also be generated using a mode-locked laser synchronized to the electrical LO source [Fig. 1(b)] [19]. This approach can be considered from either a frequency- or a time-domain perspective. From the frequency-domain view, the mode-locked laser output consists of a series of spectral lines with spacing equal to the pulse repetition frequency $f_{\rm LO}$. When this spectral comb is mixed with the RF signal in the modulator, a series of signals are generated at IF frequencies $f_{\rm IF} = f_{\rm RF} - n \cdot f_{\rm LO}$, where n is an integer, as well as at the harmonic and intermodulation frequencies. Hence, this approach can be thought of as optical heterodyning [22] with a frequency comb instead of the typical pair of optical frequencies. From the time-domain perspective, the mode-locked laser consists of a series of short optical pulses with temporal spacing of $1/f_{\rm LO}$. As the pulses are transmitted through the modulator, the RF signal is optically down-sampled via the modulator's transfer characteristic. The modulated pulses can then be detected and low-pass filtered to extract the undersampled IF signal at frequency $f_{\rm IF} = f_{\rm RF} - N \cdot f_{\rm LO}$, where N is the integer that satisfies the Nyquist criterion (i.e., $f_{\rm IF} < \cdot f_{\rm LO}/2$). A main limitation of using a mode-locked laser for down-conversion is that the instantaneous bandwidth of the RF signal must be less than half the pulse repetition rate to satisfy Nyquist. Also, when using a single-output modulator to perform the sampling operation: 1) intermodulation products are generated by the modulator's sinusoidal transmission characteristic and 2) laser amplitude noise can degrade the system noise performance.

In the next section, we describe the use of phase-encoded sampling to improve the linearity and laser noise suppression of the optical down-sampling technique.

III. Optical-Sampling System Description

The optical sampling system (Fig. 2) consists of a harmonically mode-locked fiber ring laser generating 30-ps pulses

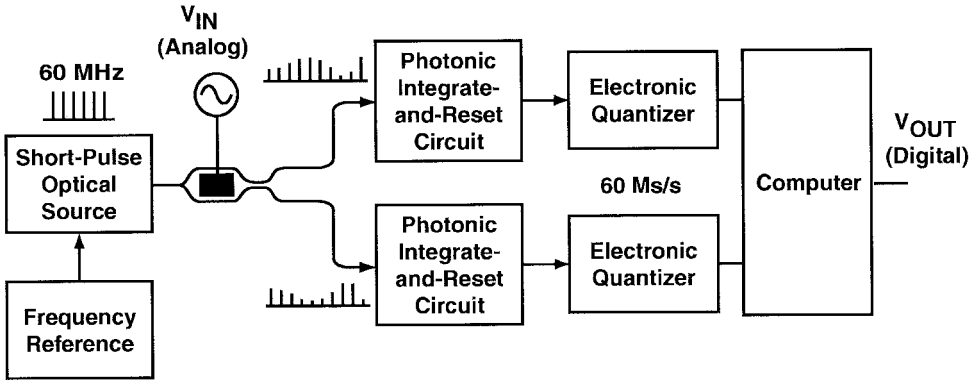

Fig. 2. Phase-encoded optical sampling system consisting of a short-pulse (30 ps) optical source, a dual-output $LiNbO_3$ Mach–Zehnder modulator, a pair of PHIR circuits, a pair of electronic quantizers (AD6644), and a computer.

at a 60-MHz rate (sixth harmonic), a dual-output $LiNbO_3$ Mach–Zehnder (MZ) modulator, and a pair of photonic integrate-and-reset (PHIR) circuits followed by 14-bit electronic quantizers (Analog Devices AD6644) operating at 60 MS/s. Two different MZ modulators having traveling-wave electrodes were used in the experiments reported here. The 3-dB bandwidth and half-wave voltage (V_π) of the two modulators are: 1) 3 GHz, 3 V and 2) 10 GHz, 11 V. The PHIR circuits convert the energy of the 30-ps pulses into slowly varying voltage signals by integrating photogenenerated current over a 10-ns interval. The digital samples from each quantizer are stored in 1-Msample buffers and then processed offline. System timing signals are derived from the detected laser output and are distributed to the PHIR circuits and the quantizers. Additional details on the system can be found in [6].

Phase-encoded optical sampling of the electrical signal is achieved by transmitting the laser-pulse train through the dual-output MZ modulator. The energy of each input pulse is interferometrically split between the two output ports. The splitting ratio is determined by the voltage applied during the time that the pulse traverses the modulator. When an MZ modulator with velocity-matched traveling-wave electrodes is used, the pulse travels through the optical waveguide at the same velocity that the electrical signal travels along the electrode. Thus, the pulse samples the applied voltage at the instant that it enters the active section of the modulator. The optical pulses are then detected and conditioned by the PHIR circuits and digitized by the electronic quantizers. After digitization, the complementary modulator output samples are combined to invert the modulator's transfer function and obtain the phase difference in the interferometer arms at the time of pulse transmission. This phase difference is linearly related to the applied analog voltage. Details of the phase-decoding process are given in [5] and [6].

By combining the information from both outputs of the MZ modulator, the phase-encoded optical sampling technique provides both high linearity and large suppression of laser amplitude noise. These performance enhancements are illustrated by the power spectra in Fig. 3 that were obtained by sampling a 28.4-MHz sinusoid using the 60-MS/s optical sampling system. For this measurement, the modulation index ($m = V_{IN,P-P}/V_\pi$) was very large (50%) and the optical

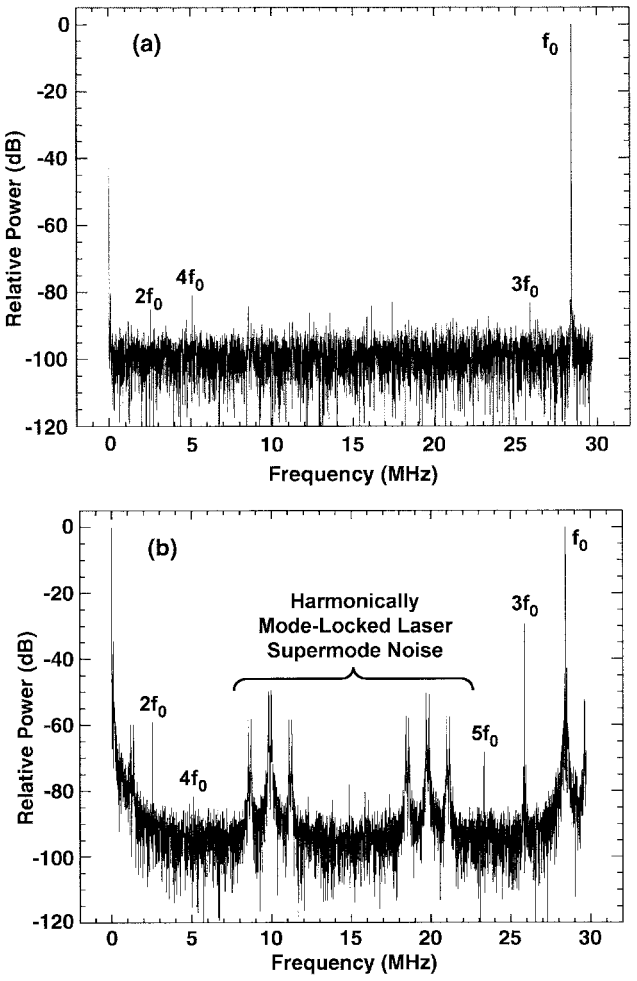

Fig. 3. Power spectra of a 28.4-MHz sinusoidal signal sampled using (a) phase-encoded optical sampling and (b) intensity sampling. The modulation index ($m = V_{\mathrm{IN},P-P}/V\pi$) was 50% and the optical power at the modulator input was 4 mW.

power at the modulator input was 4 mW. The signal-to-noise ratio (SNR) and spurious-free dynamic range (SFDR) for the phase-encoded sampled spectrum [Fig. 3(a)] are 60 dB (9.7 effective bits) and 80 dB, respectively. When only one modulator output is processed, a technique referred to as

intensity sampling [Fig. 3(b)], the SFDR decreases by 50 dB due to the harmonics generated by the modulator's sinusoidal transmission characteristic and the large modulation index used. The discrete spurs and intermodulation products centered near 10 and 20 MHz are associated with the supermode amplitude noise of the harmonically mode-locked laser [23], which has a fundamental cavity frequency of 9.9 MHz. The complex character of the supermode intermodulation spurs results from the combination of spectral aliasing and the frequency mixing of the input signal, the supermodes, and the laser relaxation oscillations in the sampling modulator. These supermode intermodulation products dominate the 33-dB reduction in the signal-to-noise-and-distortion ratio of the intensity-sampled data relative to the phase-encoded sampled data. The increase of the broadband noise floor is less than 10 dB for the intensity-sampled data. In another linearity demonstration, we obtained a two-tone third-order intermodulation-free dynamic range of 87 dB for $m = 15\%$ [24]. This result represents a 40-dB improvement over the linearity of the single-output MZ sampling approach. The linearity of the technique is limited only by the linearity of the linear electrooptic effect in a material such as $LiNbO_3$ and the temporal width of the optical sampling pulses, as discussed below. The differential detection and normalization inherent in the phase-decoding process has been demonstrated to suppress the laser amplitude noise by at least 60 dB [11].

IV. Frequency Response Investigation

The analog bandwidth of the optical sampling technique is determined entirely by the bandwidth of the electrooptic sampling modulator and the temporal width of the optical sampling pulses. The bandwidth of the sampling modulator is limited by a number of factors including electrode capacitance, velocity mismatch between the electrical signal and the optical pulse signal, electrical signal attenuation due to conductor loss (i.e., skin effect), dielectric loss, radiation loss, and packaging and connector parasitics. $LiNbO_3$ Mach–Zehnder modulators having more than 30-GHz bandwidth are commercially available [25], and polymer modulators with bandwidths exceeding 100 GHz have been demonstrated in the laboratory [26].

The analog bandwidth is also limited by the optical pulse width. For optical sampling systems that use integrate-and-reset detection, the sampled electrical-signal information is contained in the energy of the optical pulse at the output of the sampling transducer. Assuming a velocity-matched traveling-wave electrode, the transmitted pulse energy is equal to

$$E(t_0) = \int p(t - t_0)T(t)dt \tag{1}$$

where $p(t)$ is the instantaneous optical pulse power, t_0 is the time that the pulse entered the modulator, and $T(t)$ is the optical transmission of the sampling modulator, which is a function of the applied voltage being measured. Consider the sampling of a sinusoidal electrical signal. When the pulse width is much less than the signal period, the transmission is approximately constant over the pulse width and the transmitted pulse energy provides a good measure of the electrical signal the sampling instant t_0. As the pulse width approaches the signal period, the sampling process integrates variations in the transmission and the output pulse energy becomes constant, independent of the sampling time t_0 (i.e., there is no sampling). The dependence of the frequency response of the optical sampling process on the optical pulse width was investigated using a numerical simulation that includes pulse-width effects via (1). As anticipated, the analog bandwidth was found to be inversely proportional to the pulse width. For a Gaussian optical pulse having a temporal full-width at half-maximum of τ, the 3-dB bandwidth due to the pulse width is equal to $0.312/\tau$.

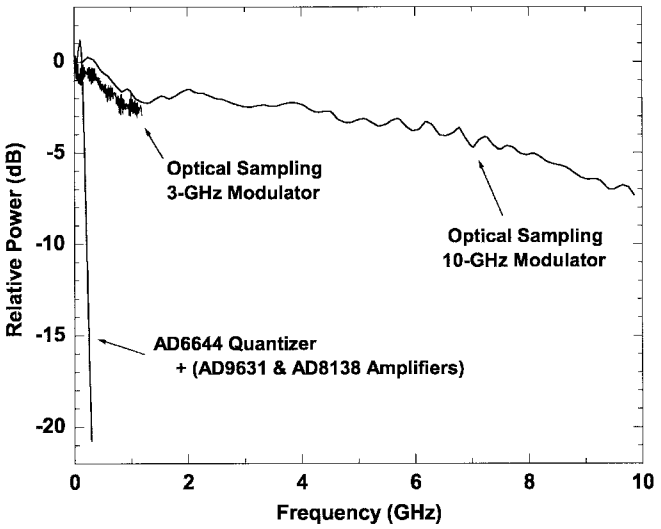

Fig. 4. Comparison of the frequency responses of an analog devices AD6644 analog-to-digital converter and the optical sampling system with both 3- and 10-GHz bandwidth sampling modulators. The signal input to the AD6644 is conditioned using AD9631 and AD8138 amplifiers in series.

We note that the analog bandwidth is limited by neither the photodetector bandwidth nor the electronic quantizer bandwidth when integrate-and-reset detection is used. In this detection scheme, the pulse energy is converted to a slowly varying voltage through the photodetection and integration processes. For our system, the integration period is much longer (10 ns) than the optical pulse width (30 ps). The quantizer operates on a voltage that is proportional to the integrated pulse energy and not instantaneous pulse power, greatly relaxing the timing accuracy requirement at the quantizer. Thus, the aperture jitter of the optical sampling system is dominated by the timing jitter of the mode-locked laser pulses as the pulses pass through the sampling modulator.

To demonstrate the wide analog bandwidth of the optical sampling technique, stepped-frequency (10 MHz to 10 GHz) measurements were performed. Fig. 4 shows the optical sampling system response for both the 3- and 10-GHz modulators. The 3-dB bandwidth of the optical sampling system with the 3- and 10-GHz modulator is 1.2 and 5 GHz, respectively. The initial, steep amplitude decrease in the responses for both modulators ($f < 1$ GHz) is attributed to the impedance transformer at the electrical input of the modulator. Also shown in Fig. 4 is the measured frequency response of the AD6644 electronic quantizers that are used in the optical sampling system. The AD6644 input was conditioned using an AD9631 unity-gain buffer and an AD8138 differential amplifier (gain$= 2$). The data of Fig. 4

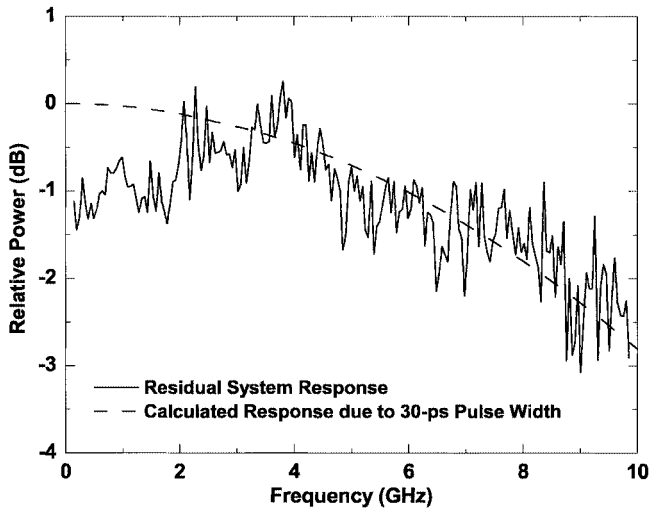

Fig. 5. Residual frequency response of the optical sampling system (solid line) after removing the frequency response of the 10-GHz dual-output modulator. The calculated response due to the 30-ps pulse width is also shown (dotted line).

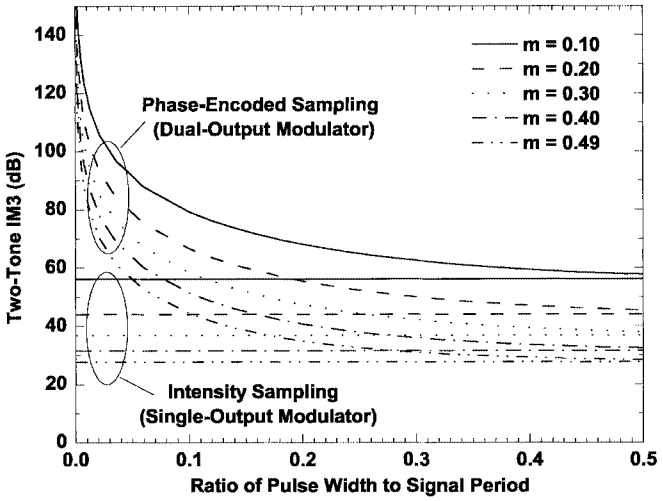

Fig. 6. Calculated dependence of system linearity on the relative optical pulse-width and the modulation index for both phase-encoded optical sampling and intensity sampling. IM3= two-tone third-order intermodulation-free dynamic range.

show that the quantizer has a 3-dB bandwidth of 160 MHz and a sharp rolloff (18 dB/octave). The overall quantizer bandwidth is primarily limited by the bandwidth of the AD8138 amplifier. It is important to note that the bandwidth of the electronic quantizer does not limit the analog bandwidth of the optical sampling system.

To separate the bandwidth limit due to the modulator from that due to the pulse width, the modulator frequency response was independently measured using an HP8510 network analyzer in conjunction with a 1550-nm laser and a 40-GHz-bandwidth photodetector. The residual system frequency response was then obtained by normalizing the measured response (Fig. 4) by the modulator frequency response. Fig. 5 shows the residual response of the system obtained from measurements with the 10-GHz modulator installed. Also shown is the simulated frequency response associated with the finite sampling aperture of a 30-ps Gaussian pulse. The good agreement between the residual system response and the pulse-width dependence at high frequency reveals that the modulator and the pulse width are the primary factors limiting the analog bandwidth. The discrepancy at low frequency (<2 GHz) is currently under investigation. The 30-ps pulse width imposes a 3-dB bandwidth of 10.4 GHz. Although the minimum pulse-width of our laser was limited to 30 ps by the laser design, high-repetition-rate mode-locked lasers producing picosecond and subpicosecond pulses have been reported [12], [27], [28]. The 850-fs pulses reported in [28] would increase the pulse-width-limited bandwidth to 370 GHz.

The SNR for an input-signal frequency of 10 GHz was measured to be 50 dB, indicating that the pulse-to-pulse laser timing jitter is less than 50 fs in agreement with previous measurements [11]. This jitter measure is an upper bound since it contains amplitude and phase noise contributions from the synthesizer used to generate the 10-GHz electrical test signal.

In addition to the amplitude response's being limited by the sampling pulse width, the *linearity* of the phase-encoded optical sampling technique is also limited by the temporal width of the optical pulses relative to the period of the signal being sampled. This limitation arises because the finite-width pulse effectively integrates the phase of the signal being sampled. When the pulses from the two modulator outputs are processed to invert the modulator's transfer function (see [6]), the integrated phase introduces a nonlinearity. We investigated the dependence of the sampling linearity on the pulse width by calculating the two-tone third-order intermodulation-free dynamic range (IM3) as a function of the ratio of the pulse width to the signal period. The analysis omitted all sources of nonlinearity except for that associated with the interferometric sampling modulator. Fig. 6 shows the results of these calculations for several modulation indexes m for both phase-encoded sampling and intensity sampling. For the intensity sampling case, the two-tone IM3 decreases with increasing modulation index due to the nonlinearity inherent in the sinusoidal transfer function of a single output of the interferometer, but the IM3 is independent of the pulse width. When phase-encoded sampling is used, the two-tone IM3 is infinite, independent of modulation index, for a zero-width sampling pulse (delta function) since we have assumed that the phase-modulation process is perfectly linear. However, for the finite-width pulses, the IM3 is a strong function of pulse width. As the pulse width increases, the linearity of the phase-encoded sampling technique approaches that of the intensity sampling technique.

Although the optical sampling system's electronics do not limit the maximum detectable signal frequency, the electronics do impose a limit on the receiver's *instantaneous* bandwidth. For the system in Fig. 2 operating at 60 MS/s, the instantaneous bandwidth is limited to the 30-MHz Nyquist bandwidth. The instantaneous bandwidth of the optical sampling technique can be extended by distributing the postsampling pulses to a parallel array of N detection circuits and time-interleaved quantizers. Using optical time-division demultiplexers to perform the pulse distribution, we have extended the instantaneous bandwidth to 104 MHz ($N = 4$) [24] and 252 MHz ($N = 8$) [6].

V. Chirp Down-Sampling Results

In a conventional Nyquist sampling system, the signal being measured is filtered prior to the sampling operation to ensure that the signal's maximum frequency component is less than half the sampling frequency. However, wide-band signals having total frequency excursion much greater than the Nyquist bandwidth can be sampled and digitally processed provided that 1) the analog bandwidth of the system is sufficiently large and 2) the instantaneous bandwidth of the signal is smaller than the system's Nyquist bandwidth. Signal frequencies greater than the Nyquist frequency of the back-end quantizers are aliased into the Nyquist bandwidth. One such wide-band signal is the linear-FM chirp waveform commonly used in radar ranging systems that incorporate "stretch" processing. The total frequency excursion of a chirped waveform may be multigigahertz, but the instantaneous bandwidth is limited to only a few megahertz. In linear-FM stretch processing, the received waveform is correlated with a delayed replica of the transmitted signal in the analog domain to reduce the signal bandwidth to be smaller than the system's ADC Nyquist bandwidth. If the chirped waveform can be directly sampled, this correlation function can be performed in the digital domain. In this section, we show that both wide-band linear- and nonlinear-FM chirp waveforms can be optically down-sampled and processed across multiple Nyquist frequency intervals.

The linear-FM chirp waveform was generated by an arbitrary-waveform generator (Tektronix AWG610). The waveform was chirped at a rate of 31.25 GHz/s from 0 to 250 MHz (8-ms duration) and had a constant power level of $+4$ dBm. Approximately two complete cycles of the waveform could be stored in the 1-Msample buffer on the AD6644 quantizer board. The signal was sampled using the 3-GHz-bandwidth modulator.

Fig. 7(a) contains a time-frequency-intensity plot of one cycle of the sampled chirp signal after phase decoding was performed. The white zigzag line shows the signal's frequency variation as it aliases through the 30-MHz Nyquist bandwidth about 8.3 times. The faint horizontal lines are evidence of constant-frequency system spurs that are about 60 dB below the signal tone. Without performing the phase-decoding operation [Fig. 7(b)], the data also exhibit 1) intense constant-frequency spurs (30 dB below the signal) near 10 and 20 MHz associated with supermode intensity noise of the harmonically mode-locked laser [23] and 2) higher order zigzag lines (barely discernable above the noise floor) due to harmonics of the sampled signal. Note that the relative level of the supermode spurs (-30 dB in this case) is a function of the amplitude of the applied electrical signal and is not a direct measure of the supermode suppression ratio (SMSR) of the laser. The SMSR of our mode-locked fiber laser is greater than 50 dB under normal operation. As mentioned above, the phase-encoded optical sampling technique greatly suppresses the effects of laser amplitude noise and improves the system linearity.

The sampled linear-chirp waveform was digitally correlated by multiplying it by an ideal chirped local-oscillator waveform

$$x_{\mathrm{LO}}(t) = \sin\left[2\pi\left(\frac{C\,t}{2} + f_0 + f_{\mathrm{IF}}\right)\,t\right] \qquad (2)$$

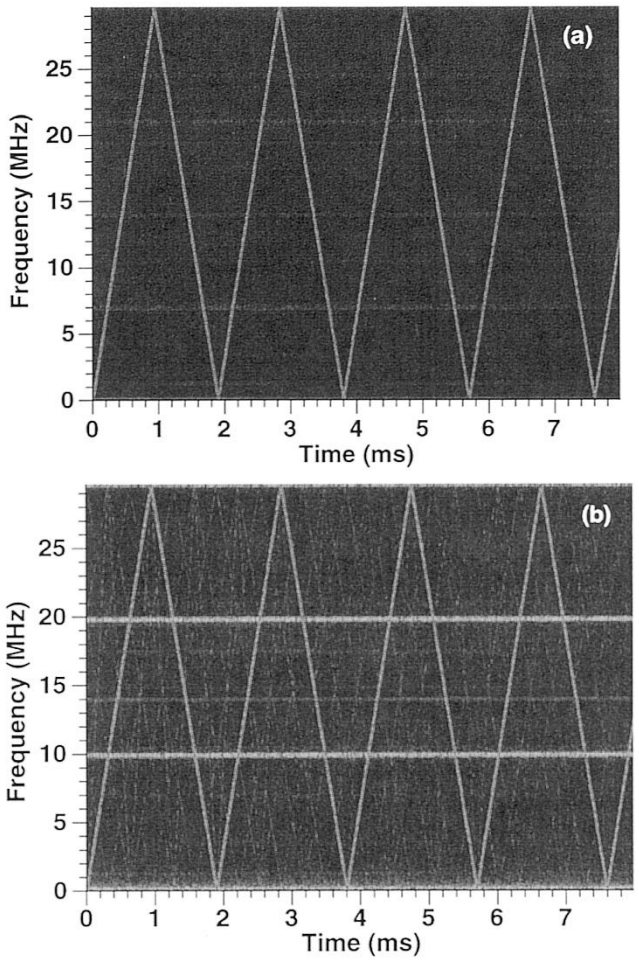

Fig. 7. Time-frequency-intensity plots of a linear-chirp waveform optically down-sampled at a 60-MS/s rate: (a) after phase decoding and (b) single-output intensity sampling without phase decoding. Chirp parameters: center frequency 125 MHz, bandwidth$= 250$ MHz, duration $= 8$ ms.

where C is the chirp rate (Hz/s), f_0 is the initial frequency, and f_{IF} is the desired intermediate frequency. Following the multiplication operation, a sliding-window fast-Fourier-transform (FFT) was applied to the data to calculate the phase evolution of the de-chirped signal. The IF frequency was chosen to place the dechirped signal in the center of an FFT frequency bin. The phase of the IF signal was then extracted from the complex FFT data. Fig. 8 shows the phase deviation between the dechirped signal and a residual-phase quadratic for a near-optimum set of parameters ($C = 31.25$ GHz/s, $f_0 = 6975$ Hz). The relatively small phase-error (3.5 degrees rms) reveals that the chirped waveform generated by the AWG610 is well described by the linear chirp expression given in (2). The residual phase-error fluctuations are thought to be related to the AWG610 since they are not correlated with Nyquist interval periodicity of the chirped signal. The requested AWG610 chirp rate was nearly identical to the empirically fit chirp rate of $C = 31.25$ GHz/s. Most importantly, this result shows that an optically sampled chirped waveform can be processed over multiple Nyquist intervals.

The wide-band down-sampling technique was also applied to a nonlinear-FM chirp waveform generated by a Miteq mi-

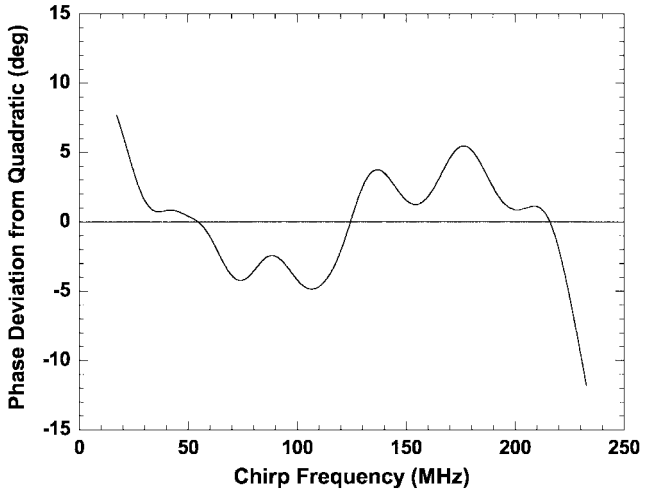

Fig. 8. Residual phase-error between an optically sampled 250-MHz linear-chirp waveform and an ideal linear-chirp waveform as a function of instantaneous chirp frequency. The rms residual error is 3.5°.

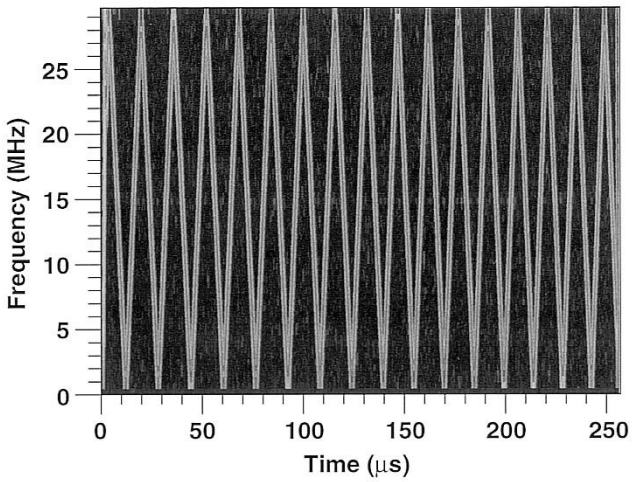

Fig. 9. Time-frequency-intensity plot of a nonlinear-chirp waveform down-sampled at a 60-MS/s rate using phase-encoded optical sampling. Chirp parameters: center frequency = 10 GHz, bandwidth = 1 GHz, duration = 256 μs.

crowave voltage-controlled oscillator (VCO) that was driven by a linear voltage-ramp generator. The resulting waveform was chirped from 9.5 to 10.5 GHz over a 256-μs duration and had a power level of +13 dBm. The chirped waveform was sampled using the 10-GHz-bandwidth modulator.

Fig. 9 contains a time-frequency intensity plot of one cycle of the sampled chirp signal after phase decoding was performed. The white zigzag line shows the signal's frequency variation as it aliases through the 30-MHz Nyquist bandwidth about 33 times.

The chirp rate of the sampled waveform was estimated by computing the slope (df/dt) of the data in Fig. 9. The rate-versus-time data (Fig. 10) reveal that the chirp rate is not constant, implying a nonlinear chirp. A static measurement of the VCO voltage-to-frequency (v-to-f) characteristic was obtained by stepping its input voltage and measuring the output frequency using a spectrum analyzer. Combining this v-to-f data with

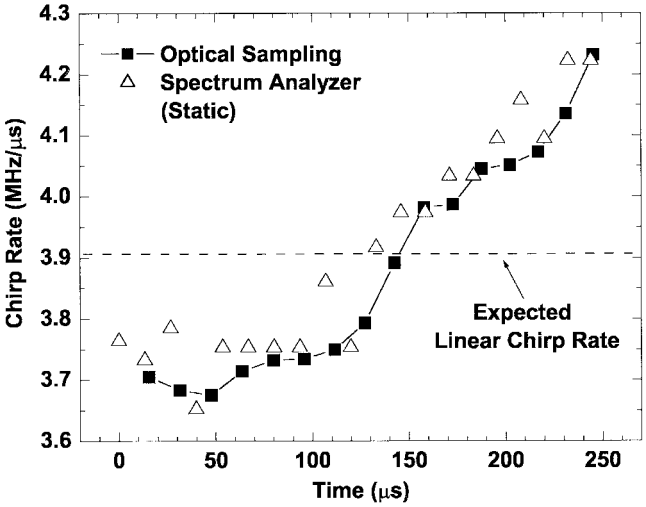

Fig. 10. Chirp rate versus time of a 1-GHz-bandwidth nonlinear-chirp waveform estimated using 1) phase-encoded optical sampling and Fourier analysis (squares and solid line) and 2) combination of static voltage-to-frequency and voltage ramp measurements (triangles). The expected linear chirp rate also shown (dotted).

a measurement of the voltage ramp provided the estimate of rate-versus-time shown in Fig. 10. Note that the two measurements agree quite well.

In this section, we have shown that wide-band electrical signals can be optically down-sampled and processed across multiple Nyquist intervals. It is worth noting two points. First, the undersampling operation does not violate the Nyquist criterion since the instantaneous bandwidth of the chirp signals is less than the Nyquist sampling bandwidth. Second, in addition to aliasing the wide-band signal, the undersampling operation also aliases all of the noise within the system's analog bandwidth into the Nyquist bandwidth. This aliased noise will limit the sensitivity of the sampling system. Thus, this aliased down-sampling technique is useful as an instrument to measure the amplitude and phase characteristics of wide-band waveforms having high SNR. It will be less useful in linear-FM radar receivers operating on low-SNR signals and on signals having range-extent bandwidth that exceeds the Nyquist bandwidth.

VI. Conclusion

In this paper, we have demonstrated that phase-encoded optical sampling allows wide-band radio-frequency and microwave signals to be frequency down-converted and digitized in a single operation with high fidelity. Both linear- and nonlinear-FM chirp waveforms have been sampled and analyzed digitally. The 3-dB analog bandwidth of our current system is limited to 5 GHz by the combination of the bandwidth of the sampling modulator and the aperture-related bandwidth of the 30-ps sampling pulses. Analog bandwidths in excess of 100 GHz should be feasible based on reported modulator and mode-locked laser technology. We note that the timing jitter of the mode-locked laser ultimately limits the maximum achievable SNR of the down-sampled signal for high input frequencies.

ACKNOWLEDGMENT

The authors would like to acknowledge useful technical discussions with R. C. Williamson. They would also like to thank G. McGrew and T. Sangiolo for the loan of the X-band 1-GHz chirp generator, and H. Crombie of Tektronix for the loan of the AWG610 arbitrary waveform generator.

REFERENCES

[1] R. H. Walden, "Analog-to-digital converter survey and analysis," *IEEE J. Select. Areas Commun.*, vol. 17, pp. 539–549, 1999.
[2] *Analog Devices AD7674 Specification Sheet*, 2002.
[3] *Analog Devices AD6645 Specification Sheet*, 2002.
[4] *Maxim MAX108 Specification Sheet*, 2001.
[5] J. C. Twichell and R. Helkey, "Phase-encoded optical sampling for analog-to-digital converters," *IEEE Photon. Technol. Lett.*, vol. 12, pp. 1237–1239, 2000.
[6] P. W. Juodawlkis, J. C. Twichell, G. E. Betts, J. J. Hargreaves, R. D. Younger, J. L. Wasserman, F. J. O'Donnell, K. G. Ray, and R. C. Williamson, "Optically sampled analog-to-digital converters," *IEEE Trans. Microwave Theory Tech.*, vol. 49, pp. 1840–1852, 2001.
[7] T. R. Clark, J. U. Kang, and R. D. Esman, "Performance of a time- and wavelength-interleaved photonic sampler for analog-digital conversion," *IEEE Photon. Technol. Lett.*, vol. 11, pp. 1168–1170, 1999.
[8] F. Coppinger, A. S. Bhushan, and B. Jalali, "12 Gsample/s wavelength division sampling analogue-to-digital converter," *Electron. Lett.*, vol. 36, pp. 316–318, 2000.
[9] W. Ng, R. Stephens, D. Persechini, and K. V. Reddy, "Ultra-low jitter modelocking of Er-fiber laser at 10 GHz and its application in photonic sampling for analogue-to-digital conversion," *Electron. Lett.*, vol. 37, pp. 113–115, 2001.
[10] T. R. Clark, T. F. Carruthers, P. J. Matthews, and I. N. Duling III, "Phase-noise measurements of ultrastable 10 GHz harmonically mode-locked fiber laser," *Electron. Lett.*, vol. 35, pp. 720–721, 1999.
[11] P. W. Juodawlkis, J. C. Twichell, J. L. Wasserman, G. E. Betts, and R. C. Williamson, "Measurement of mode-locked laser timing jitter by use of phase-encoded optical sampling," *Opt. Lett.*, vol. 26, pp. 289–291, 2001.
[12] C. M. DePriest, T. Yilmaz, A. Braun, J. H. Abeles, and P. J. Delfyett Jr., "High-quality photonic sampling streams from a semiconductor diode ring laser," *IEEE J. Quantum. Electron.*, vol. 38, pp. 380–389, 2002.
[13] L. A. Jiang, S. T. Wong, M. E. Grein, E. P. Ippen, and H. A. Haus, "Measuring timing jitter with optical cross correlations," *IEEE J. Select. Topics Quantum Electron.*, vol. 38, pp. 1047–1052, 2002.
[14] B. H. Kolner and D. W. Dolfi, "Intermodulation distortion and compression in an integrated electrooptic modulator," *Appl. Opt.*, vol. 26, pp. 3676–3680, 1987.
[15] G. K. Gopalakrishnan, W. K. Burns, and C. H. Bulmer, "Microwave-optical mixing in $LiNbO_3$ modulators," *IEEE Trans. Microwave Theory Tech.*, vol. 41, pp. 2383–2391, 1993.
[16] A. C. Lindsay, G. A. Knight, and S. T. Winnall, "Photonic mixers for wide bandwidth RF receiver applications," *IEEE Trans. Microwave Theory Tech.*, vol. 43, pp. 2311–2317, 1993.
[17] K. J. Williams and R. D. Esman, "Optically amplified downconverting link with shot-noise-limited performance," *IEEE Photon. Technol. Lett.*, vol. 8, pp. 148–150, 1996.
[18] C.-K. Sun, R. J. Orazi, and S. A. Pappert, "Efficient microwave frequency conversion using photonic link signal mixing," *IEEE Photon. Technol. Lett.*, vol. 8, pp. 154–156, 1996.
[19] C. H. von Helmolt, U. Krüger, and K. Krüger, "Microwave fiber-optic downconverter," in *Proc. Conf. Optical Fiber Communications (OFC)*, 1997, pp. 357–358.
[20] R. Helkey, J. C. Twichell, and C. I. Cox, "A down-conversion optical link with RF gain," *IEEE J. Lightwave Technol.*, vol. 15, pp. 956–961, 1997.
[21] J. T. Gallo and J. K. Godshall, "Comparison of series and parallel optical modulators for microwave down-conversion," *IEEE Photon. Technol. Lett.*, vol. 10, pp. 1623–1625, 1998.
[22] S. A. Pappert, R. Helkey, and R. T. Logan Jr., "Photonic link techniques for microwave frequency conversion," in *RF Photonic Technology in Optical Fiber Links*, W. S. C. Chang, Ed. Cambridge, U.K.: Cambridge Univ. Press, 2002, pp. 293–333.
[23] F. Rana, H. L. T. Lee, R. J. Ram, M. E. Grein, L. A. Jiang, E. P. Ippen, and H. A. Haus, "Characterization of the noise and correlations in harmonically mode-locked lasers," *J. Opt. Soc. Amer. B*, vol. 19, pp. 2609–2621, 2002.
[24] J. C. Twichell, J. L. Wasserman, P. W. Juodawlkis, G. E. Betts, and R. C. Williamson, "High-linearity 208-MS/s photonic analog-to-digital converter using 1-to-4 optical time-division demultiplexers," *IEEE Photon. Technol. Lett.*, vol. 13, pp. 714–716, 2001.
[25] *JDS Uniphase OC-768, 40-Gb/s Amplitude Modulator Specification Sheet*, 2002.
[26] D. Chen, H. R. Fetterman, A. Chen, W. H. Steier, L. R. Dalton, W. Wang, and Y. Shi, "Demonstration of 110 GHz electro-optic polymer modulators," *Appl. Phys. Lett.*, vol. 70, pp. 3335–3337, 1997.
[27] T. F. Carruthers, I. N. Duling III, M. Horowitz, and C. R. Menyuk, "Dispersion management in a harmonically mode-locked fiber soliton laser," *Opt. Lett.*, vol. 25, pp. 153–155, 2000.
[28] M. Nakazawa, "A 40-GHz 850-fs regeneratively FM mode-locked polarization-maintaining erbium fiber ring laser," *IEEE Photon. Technol. Lett.*, vol. 12, pp. 1613–1615, 2000.

Paul W. Juodawlkis (S'86–M'86) received the B.S. degree in electrical engineering *(summa cum laude)* from Michigan Technological University, Houghton, in 1986, the M.S. degree in electrical engineering from Purdue University, West Lafayette, IN, in 1988, and the Ph.D. degree in electrical engineering from the Georgia Institute of Technology, Atlanta, in 1999.

His doctoral dissertation concerned the ultrafast optoelectronic properties and device applications of low-temperature-grown semiconductor quantum-well materials. From 1988 to 1993, he was a Technical Staff Member at Lincoln Laboratory, Massachusetts Institute of Technology (MIT), Lexington, where he was a Hardware Systems Engineer on a multisensor airborne testbed program. He then joined the Ultrafast Optical Communications Laboratory (UFOCL), Georgia Institute of Technology. In 1999, he rejoined the Lincoln Laboratory, MIT, as a member of the Electro-Optic Materials and Devices Group and has been leading research on optically sampled analog-to-digital converters and semiconductor optoelectronic devices. His current research interests include laser noise characteristics, ultrashort pulse generation and applications, high-power semiconductor optical amplifiers, and quantum-well electrorefractive modulators.

Dr. Juodawlkis is currently Chair of the IEEE Lasers & Electro-Optics Society (LEOS) Technical Committee on Microwave Photonics and was Program Co-Chair for the 2003 LEOS Summer Topical Meeting on Photonic Time/Frequency Measurement and Control. He is a Member of the Optical Society of America.

Jeffrey J. Hargreaves (A'90–M'98) was born in Honolulu, HI, in 1965. He received the associate's degree in computers and electronics from New Hampshire Vocational Technical College, Concord, in 1985, the B.S. degree in electrical engineering from the University of Massachusetts, Amherst, in 1995, and the M.S. degree in electrical engineering from the University of New Hampshire, Durham, in 1999.

His master's thesis research focused on intermodulation products due to the nonlinear effects of colocated antennas. From 1985 to 1987, he was an Engineering Technician at M/A COM Inc., where he worked in the controlled components group. In 1987, he joined the Massachusetts Institute of Technology (MIT)'s Haystack Observatory as an RF Technician supporting MIT Lincoln Laboratory's Long Range Imaging Radar (LRIR) system. In 1993, he was promoted to Technical Staff Member while working on the development of low-noise receivers and frequency-generation systems for MIT Lincoln Laboratory's Haystack Auxiliary (HAX) radar. In 2000, he joined MIT Lincoln Laboratory as a Technical Staff Member in the Electro-Optic Materials and Devices group, where he is currently involved in the development of analog-to-digital converters utilizing optical sampling techniques. His research interests include phase noise characteristics of RF and optical devices, integration of optical sampling techniques into radar systems, low-noise RF sources, and nonlinear effects of receiver systems.

Mr. Hargreaves is a Member of Sigma Xi and the IEEE Lasers and Electro-Optics Society (LEOS).

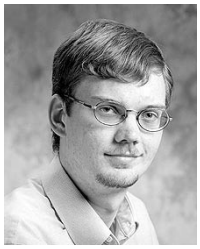

Richard D. Younger was born in Denver, CO, in 1978. He received the B.S. degree *(magna cum laude)* in engineering physics from the University of Colorado, Boulder, in 2000.

His undergraduate research accomplishments include the development of a desktop demonstration of a strongly bound charged plasma at the Center for Integrated Plasma Studies and a theoretical investigation of electron transport in quantum heterostructures at the Joint Institute for Laboratory Astrophysics. He is currently an Assistant Technical Staff member at the Lincoln Laboratory, Massachusetts Institute of Technology, working on the development of photonic analog-to-digital converters.

Gerard W. Titi (S'83–M'83), photograph and biography not available at the time of publication.

Jonathan C. Twichell (M'00) received the A.B. degree from Earlham College, Richmond, IN, in 1974. He received the M.S. and Ph.D. degrees from the University of Wisconsin-Madison in 1978 and 1984, respectively, both in nuclear engineering.

His thesis research focused on the effects of impurity generation and hydrogen recycling on energy confinement in high-energy-density magnetically confined plasmas. After teaching for three years at the University of Oklahoma, he joined the Lincoln Laboratory, Massachusetts Institute of Technology. From 1986 until 1991, he worked in the High-Energy Laser Propagation and Control group designing and implementing wavefront sensors and developing wavefront reconstruction algorithms. Between 1991 and 1998, he was a member of the Submicrometer Technology group, where he worked on diamond material physics, primarily field- and photoelectron emitters. He is currently the Leader of the Electro-Optic Materials and Devices group. His present research interests center on photonic enhancements to traditional electronic systems and the application of nonlinear systems to wideband signal processing.

Dr. Twichell is a Member of the IEEE Lasers & Electro-Optics Society (LEOS) and the American Physical Society.